Volume Title
ASP Conference Series, Vol. **Volume Number**
Author

Magnetic Fields and the Formation of Cores and Disks

Shantanu Basu,[1] Nicole D. Bailey,[1] and Wolf B. Dapp[2]

[1]*Department of Physics and Astronomy, Western University, London, Ontario N6A 3K7, Canada*

[2]*Jülich Supercomputing Centre, Institute for Advanced Simulation, FZ Jülich, Germany*

Abstract. We review recent results of non-ideal magnetohydrodynamic models for the fragmentation of molecular clouds and the collapse of cloud cores to form protostar-disk systems. Thin-disk models can elucidate many aspects of the physical problem and allow the calculation of large dynamic range of time and length scales.

1. Introduction

A large-scale magnetic field exerts a dramatic influence on fragmentation properties of molecular clouds, especially when accounting for non-ideal magnetohydrodynamics (MHD) based on partial ionization effects. Furthermore, within a collapsing cloud core, the magnetic field assumes a crucial role in the near-protostar environment, a region where the magnetic flux problem is resolved and the angular momentum content of the forming star-disk system is finally determined.

The magnetic field is most generally invoked in star formation as an explanation for the observed very low efficiency of star formation in molecular clouds. Molecular clouds are the exclusive sites of star formation but are characterized by a very low efficiency of star formation, e.g., in the Taurus Molecular Cloud only $\sim 1\%$ of the mass is in the form of stars (Goldsmith et al. 2008), and the global rate of star formation in the Galaxy is estimated by various means to be $1 - 5\,M_\odot$ yr^{-1} (Misiriotis et al. 2006; Robitaille & Whitney 2010). This is only $\sim 1\%$ of that expected if molecular gas in the Galaxy is collapsing on its dynamical time.

Magnetic fields that create a subcritical mass-to-flux ratio are a viable means of preventing most molecular cloud material from forming stars during the lifetime of the cloud, assuming that the neutral-ion coupling is sufficiently strong. In this paper, we will frequently refer to the normalized mass-to-flux ratio $\mu \equiv 2\pi G^{1/2}\sigma_n/B_z$, where $(2\pi G^{1/2})^{-1}$ is the critical value of the mass-to-flux ratio. Clouds that are subcritical ($\mu < 1$) cannot collapse in the flux-freezing limit but more realistically undergo an ambipolar-diffusion-initiated fragmentation that occurs on a time scale many times longer than the dynamical time. Clouds that are supercritical ($\mu > 1$) will fragment rapidly on a dynamical time into Jeans mass scales. The transcritical case ($\mu \approx 1$) is a fascinating middle ground that is discussed in this paper.

We are working in the scenario that the low efficiency of star formation is explained by having most of the diffuse envelope of a molecular cloud in the form of

subcritical gas. This subcritical common envelope is not expected to lead to significant (or any) star formation during the lifetime of the molecular cloud. However, regions of the molecular cloud may become transcritical or supercritical due to accumulation of matter into the molecular cloud or nonlinear perturbations that lead to localized rapid ambipolar diffusion. These can allow fragmentation to be initiated in subregions of a molecular cloud, and lead to weak or rich clusters of stars.

Once cores have formed by a fragmentation process, they are mildly supercritical and begin runaway collapse toward formation of a central protostar. The angular momentum provides a barrier to this, with observationally determined ratios of rotational to gravitational energy $\beta \approx 10^{-4}$ still leading to the formation of large disks if angular momentum is conserved. However, even a mildly supercritical mass-to-flux ratio provides enough magnetic coupling to the core envelope that disk formation is suppressed in the flux-freezing limit. This is known as the *magnetic braking catastrophe*. We show how this problem is resolved using a detailed treatment of microphysics including a chemical network in order to calculate coefficients of Ohmic dissipation and ambipolar diffusion. Exotic explanations are not required for a small disk to form at early times.

2. Fragmentation of Magnetic Molecular Clouds

Numerical simulations in the thin-disk approximation have revealed the dramatic dependence of fragmentation properties on the ambient initial mass-to-flux ratio μ_0 (Basu et al. 2009). Unlike a uniform medium, sheets and filaments exhibit a preferred scale of fragmentation for any combination of mass (per unit area or length). When a magnetic field and partial ionization are taken into account, the regions with transcritical mass-to-flux ratio have the largest preferred fragmentation scales. This is clearly seen from the results of a linear perturbation analysis of a partially ionized sheet. Figure 1 shows the run of preferred fragmentation scale versus mass-to-flux ratio, taken from Bailey & Basu (2012) and based on the earlier results of Ciolek & Basu (2006). The peak actually occurs at $\mu_0 = 1.1$, slightly on the supercritical side, as these modes are driven by a combination of neutral-ion slip and inward dragging of field lines. The latter allows strong restoring forces to be set up due to the tension and pressure of the relatively strong magnetic field. The solid line in Figure 1 is the set of preferred wavelengths in the limit of flux freezing (neutral-ion collision time $\tau_{\rm ni,0} = 0$) and the other lines are the set of preferred wavelengths if there is partial coupling of neutrals and ions with successively decreasing ionization fraction as $\tau_{\rm ni,0}$ increases. The case $\tau_{\rm ni,0}/t_0 = 0.2$ corresponds to the canonical cosmic ray ionization rate.

Figures 2 and 3 show images of column density along with velocity vectors for fragmentation of clouds that are significantly subcritical ($\mu_0 = 0.5$), transcritical ($\mu_0 = 1.1$), somewhat supercritical ($\mu_0 = 2.0$), and significantly supercritical ($\mu_0 = 10$). All modeled regions are the same size, about 2 pc $\times$ 2 pc for typical parameters. The transcritical cloud yields the largest fragments, while the highly sub- and supercritical clouds yield the smallest ones. The latter weak magnetic field case yields the most elongated structures.

An extrapolation of these numerical results is that a cloud with a variety of mass-to-flux ratios in its various regions will develop a broad core mass function. Monte Carlo simulations of this using the linear fragmentation theory (Bailey & Basu 2013) reveal that a narrow lognormal distribution of cores in the hydrodynamic limit is transformed to a broad distribution with a shallow power-law high-mass tail in the magnetic

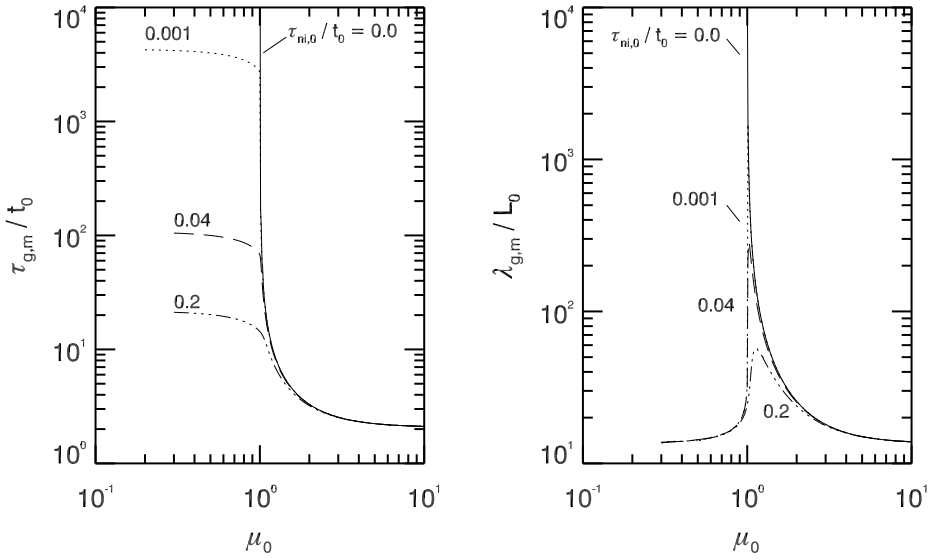

Figure 1. Left: Minimum growth time of the most gravitationally unstable mode ($\tau_{g,m}/t_0$) as a function of mass-to-flux ratio (μ_0). Right: Length scale of the most unstable mode ($\lambda_{g,m}/L_0$) as a function of μ_0. Units of time t_0 and length L_0 are described in Basu et al. (2009) and are related to the dynamical time and Jeans scale for the system. Different values of $\tau_{ni,0}$ correspond to different levels of ionization, with $\tau_{ni,0}/t_0 = 0.2$ corresponding to the canonical cosmic ray ionization rate, and $\tau_{ni,0}/t_0 = 0$ corresponding to the flux-frozen limit. From Bailey & Basu (2012).

flux-frozen case, and that the addition of ambipolar diffusion leads to a broad mass function with a high-mass cutoff.

While the thin-disk approximation is an idealization of a molecular cloud, it is motivated by the idea that while molecular clouds will in general have rarefied turbulent envelopes, the star formation will take place in embedded dense sheets and filaments with near-thermal line widths. This is illustrated theoretically by the one-dimensional simulations of turbulence propagation in a stratified atmosphere by Kudoh & Basu (2003, 2006). They show that large nonlinear motions occur in the rarefied regions but that a dense midplane region maintains transonic motions. Furthermore, three-dimensional simulations of flattened clouds without vertically propagating turbulence (Kudoh et al. 2007; Kudoh & Basu 2008, 2011) are also consistent with the results of the thin-disk simulations. We do not focus on the three-dimensional results in this paper.

The preferred fragmentation scale will also depend on the level of ionization, and in fact a dramatic drop in this quantity is expected within a molecular cloud in the region where the column density is high enough to shield out the background ultraviolet starlight. This leads to the idea of two-stage fragmentation (Bailey & Basu 2012), described as follows. One can envision two dramatic events during the assemblage of a molecular cloud. If we assume that a molecular cloud is assembled from HI cloud material that is generally subcritical (Heiles & Troland 2005) and ionized by ultraviolet (UV) starlight, then a cloud may resist fragmentation (due to the very long ambipolar diffusion time) until flows primarily along the magnetic field lines raise the mass-to-flux ratio to slightly above the critical value. At this point, the transcritical (but still UV

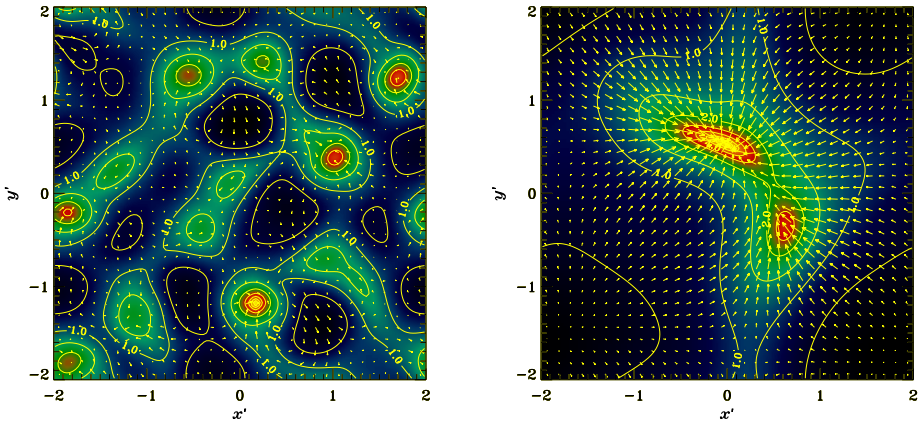

Figure 2. Image and contours of column density $\sigma_n(x, y)$ and velocity vectors of neutrals, at the time when the column density is enhanced by a factor of 10 and runaway collapse is well underway. Left: subcritical (magnetically dominated) model with $\mu_0 = 0.5$. Right: transcritical model with $\mu_0 = 1.1$. The horizontal or vertical distance between footpoints of velocity vectors corresponds to a speed of $0.5c_s$, where c_s is the isothermal sound speed. From Basu et al. (2009).

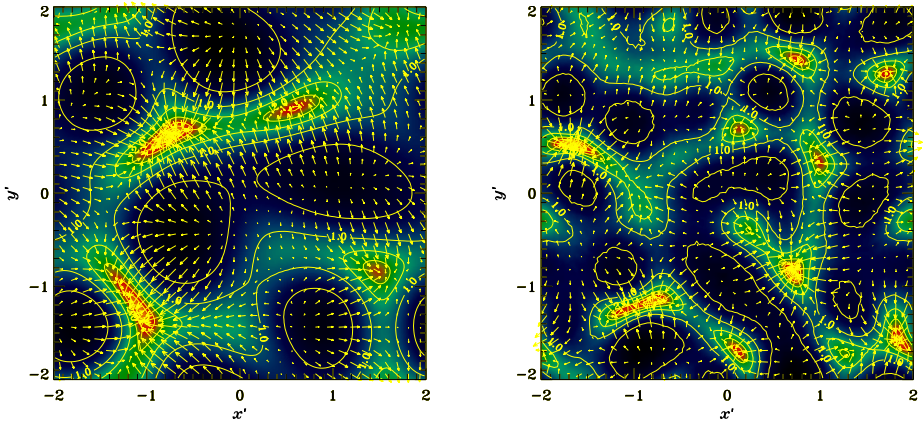

Figure 3. Same as previous figure but for different models. Left: Mildly supercritical model with $\mu_0 = 2.0$. Right: Highly supercritical model with $\mu_0 = 10$. From Basu et al. (2009).

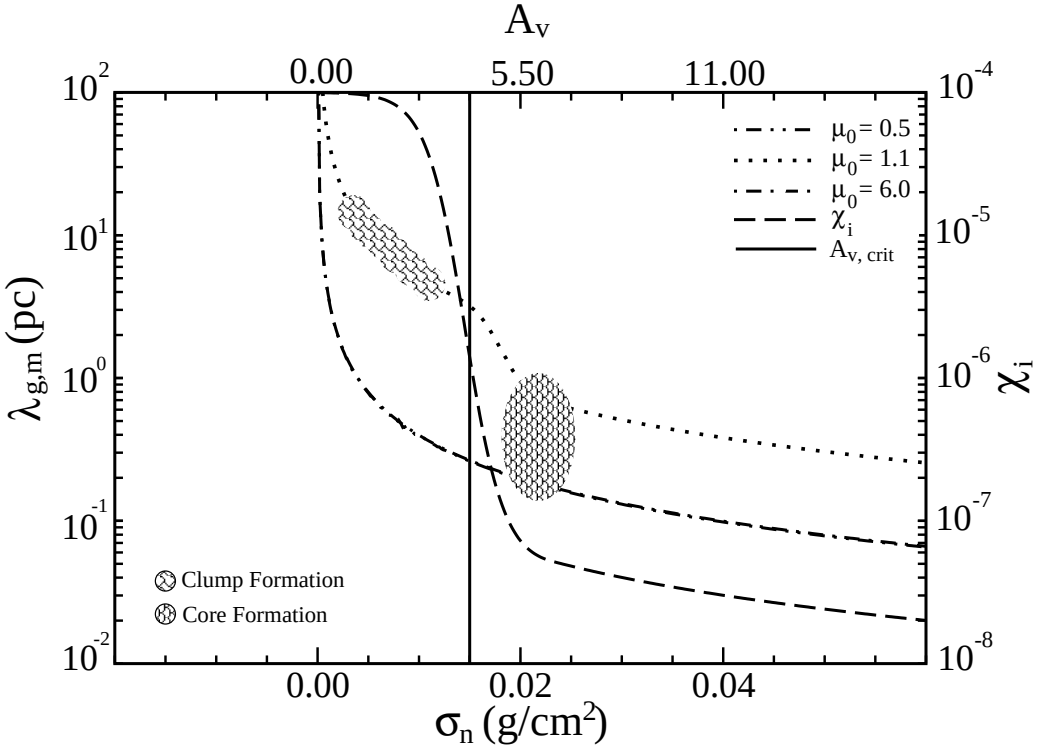

Figure 4. Illustrative plot of the two-stage fragmentation scenario. The ionization fraction χ_i versus column density is in the dashed line. The other lines show the dependence of preferred fragmentation scale on the column density for various values of μ_0. Transcritical clumps that form on the left side of the critical visual extinction $A_{v,crit}$ (vertical solid line) for ultraviolet starlight can undergo a second fragmentation event on the right side of $A_{v,crit}$ when the preferred fragmentation scale drops significantly. Shaded regions show the parameter space for the formation of clumps and cores respectively. From Bailey & Basu (2012).

ionized) cloud may form large fragments as predicted by the linear theory. As these fragments develop, they will also become more supercritical, since their evolution is partially driven by neutral-ion drift. Once the column density in the fragments also crosses the column density threshold for the transition to cosmic ray dominated ionization, the fragmentation length and time scales will drop dramatically, and a second stage of fragmentation may be possible.

Figure 4 shows a schematic picture of the two-stage fragmentation model. It plots the ionization fraction χ_i as well as the fragmentation length scale $\lambda_{g,m}$ for various values of μ_0, all as functions of column density. In the diffuse regions where clouds are just forming from subcritical gas, we expect the mass-to-flux ratio be in the transcritical ($\mu_0 \approx 1$) regime. The parameter space where we expect the fragmentation of the gas into parsec size clumps is indicated by the hatched region to the left of the critical visual extinction $A_{v,crit}$. Linear analysis reveals that the hatched region corresponds to fragmentation time scales on the order of 2-10 Myr. As the column density of the region increases, the region will cross over to the right hand side of $A_{v,crit}$. The hatched region on this side of $A_{v,crit}$ represents the parameter space for subfragmentation within

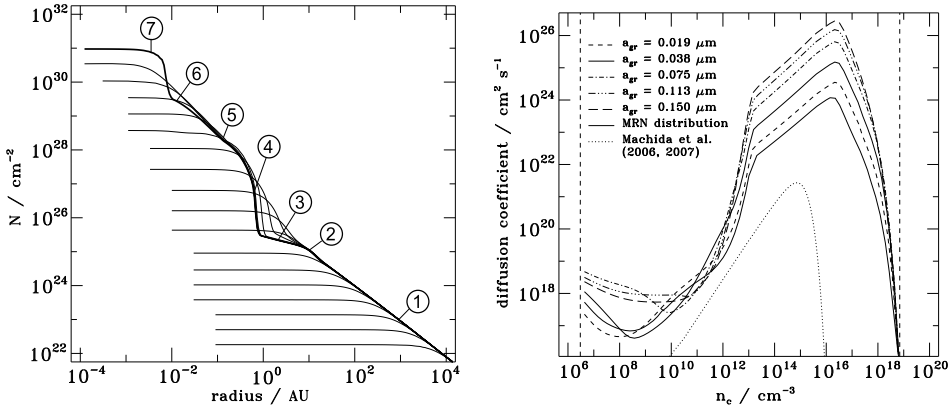

Figure 5. Left: Column number density profile versus radius for collapsing core model. The thin lines (in ascending order) are plots at successive times. Several features are identifiable via their associated breaks in the profile. (1) Prestellar infall profile with $N \propto r^{-1}$. (2) Magnetic wall at $\approx$ 10 AU, where the bunched-up field lines decelerate material before it continues the infall. (3) Expansion wave profile with $N \propto r^{-1/2}$ outside the first core. (4) First core at 1 AU. (5) Infall profile onto the second core with $N \propto r^{-1}$. After the first core has reached $\approx 1,000$ K, it starts to collapse, as H_2 is dissociated. (6) Expansion wave profile with $N \propto r^{-1/2}$ outside the second core. (7) Second core at $\approx 1\ R_\odot$. Right: Central magnetic diffusion coefficient $\eta_{\rm eff}$ versus number density for different grain sizes, extracted from the dynamical model. The vertical line at the left indicates the density at which the detailed chemistry and non-ideal MHD treatment is switched on. Beyond $n_c \approx 10^{18}$ cm^{-3} the resistivity plummets, after having already declined due to thermal ionization. This is where we switch the chemistry calculations off again, and is denoted by the vertical line on the right. Due to grain destruction, flux-freezing is restored there. Both figures from Dapp et al. (2012).

the clump. The length scales of fragmentation here are a few $\times$ 0.1 pc, roughly the size of observed dense cores. The time scales of fragmentation are also significantly shorter than the timescale of collapse for the larger parent transcritical clump. This second-stage fragmentation is expected to take place in gas that is either still transcritical or has become supercritical.

3. Core Collapse to Disk Formation

In order to form stars of the observed sizes and rotation rates, most of the angular momentum has to be removed from the infalling gas. This is the classical angular momentum problem. The required reduction of angular momentum is often credited to magnetic braking, which acts during the contraction and collapse by linking the core with its envelope and transferring angular momentum. Recent numerical simulations of protostellar collapse under the assumption of ideal MHD have suggested the converse problem, namely that cores may experience catastrophic magnetic braking. This is the result that an extremely pinched magnetic field configuration has enough strength and exerts a long enough lever arm on the inner regions of collapse that magnetic braking can suppress the formation of a centrifugal disk entirely.

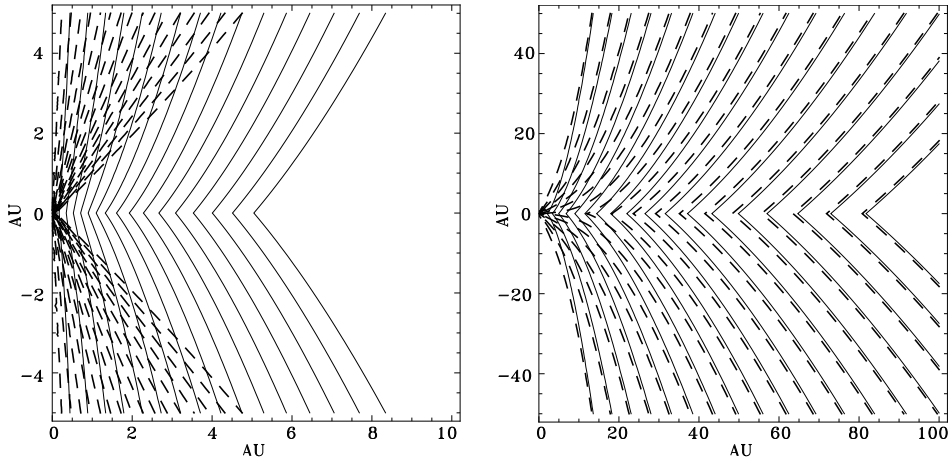

Figure 6. Magnetic field lines in the vicinity of a newly formed stellar core. The box on the left has dimensions 10 AU on each side, while the box on the right has dimensions 100 AU. Both figures from Dapp et al. (2012).

Catastrophic magnetic braking was first demonstrated by Allen et al. (2003), who used two-dimensional (2D) axisymmetric calculations. Subsequent ideal MHD simulations by Mellon & Li (2008) in 2D and Hennebelle & Fromang (2008) in three dimensions showed that catastrophic magnetic braking occurs for initially aligned (magnetic field parallel to rotation axis) rotators in which the magnetic field is strong enough that $\mu \leq 10$.

The left panel of Figure 5 shows the column number density profile versus radius at various times in the collapse process of a prestellar core (Dapp et al. 2012). Using the thin-disk approximation, the collapse is followed over a wide dynamic range of scales. A detailed chemical network model is used to calculate ionization levels and the effect of ambipolar diffusion and Ohmic dissipation. Many important features of the collapse profile are captured in this model, as described in the figure caption. The high resolution of the model allows to identify all important breaks in the profile including the presence of a double expansion wave and a magnetic wall. The right panel of Figure 5 shows the effective magnetic diffusion coefficient in the central cell, for various assumed grain sizes $a_{\rm cr}$ in the chemical network model, or for an MRN grain size distribution. The diffusivity rises steeply starting at a number density $n \approx 10^{12}$ cm^{-3}, leading to rapid magnetic diffusion and a dramatic reduction of magnetic braking. Three-dimensional simulations (Machida et al. 2006, 2007) also show very effective Ohmic dissipation in this phase of evolution.

Figure 6 shows the magnetic field lines in the model, in boxes of size 10 AU and 100 AU, respectively. The dashed lines represent the flux-freezing model, while the solid lines show *the same* field lines for the model including non-ideal MHD effects for a grain size $a_{\rm gr} = 0.038$ μm. In both cases, the second core has just formed and is on the left axis midplane. The field lines straighten out significantly on small scales in the non-ideal MHD model compared to the flux-frozen model.

Due to the magnetic diffusion and relaxed field line structure within 10 AU, magnetic braking becomes ineffective and a protostellar disk is indeed able to form very soon after the formation of the second core. The centrifugal support rises rapidly and a

low-mass disk of radius $\approx 10\,R_\odot$ is formed at the earliest stage of star formation, when the second core has mass $\sim 10^{-3}\,M_\odot$. The mass-to-flux ratio is $\sim 10^4$ times the critical value in the central region.

Estimates based on the angular momentum in the collapsing core predict that no disk larger than $\sim$ 10 AU form around Class 0 objects younger than $\sim 4 \times 10^4$ yr. This agrees well with the observations of Maury et al. (2010) who do not find evidence for disks $\gtrsim$ 50 AU in Class 0 objects. ALMA will soon allow observers to test this prediction more stringently.

Acknowledgments. We thank the organizers of the ALMA symposium for a very stimulating conference in the beautiful resort location of Hakone.

References

Allen, A., Li, Z.-Y., & Shu, F. H. 2003, ApJ, 599, 363. arXiv:astro-ph/0311377
Bailey, N. D., & Basu, S. 2012, ApJ, 761, 67. 1209.4664
— 2013, ApJ, 766, 27. 1301.7300
Basu, S., Ciolek, G. E., & Wurster, J. 2009, NewA, 14, 221. 0806.2482
Ciolek, G. E., & Basu, S. 2006, ApJ, 652, 442. arXiv:astro-ph/0607622
Dapp, W. B., Basu, S., & Kunz, M. W. 2012, A&A, 541, A35. 1112.3801
Goldsmith, P. F., Heyer, M., Narayanan, G., Snell, R., Li, D., & Brunt, C. 2008, ApJ, 680, 428. 0802.2206
Heiles, C., & Troland, T. H. 2005, ApJ, 624, 773. arXiv:astro-ph/0501482
Hennebelle, P., & Fromang, S. 2008, A&A, 477, 9. 0709.2886
Kudoh, T., & Basu, S. 2003, ApJ, 595, 842. arXiv:astro-ph/0306473
— 2006, ApJ, 642, 270. arXiv:astro-ph/0601072
— 2008, ApJ, 679, L97. 0804.4303
— 2011, ApJ, 728, 123. 1012.5707
Kudoh, T., Basu, S., Ogata, Y., & Yabe, T. 2007, MNRAS, 380, 499. 0706.2696
Machida, M. N., Inutsuka, S.-i., & Matsumoto, T. 2006, ApJ, 647, L151. arXiv:astro-ph/0603456
— 2007, ApJ, 670, 1198. arXiv:astro-ph/0702183
Maury, A. J., André, P., Hennebelle, P., Motte, F., Stamatellos, D., Bate, M., Belloche, A., Duchêne, G., & Whitworth, A. 2010, A&A, 512, A40. 1001.3691
Mellon, R. R., & Li, Z.-Y. 2008, ApJ, 681, 1356. 0709.0445
Misiriotis, A., Xilouris, E. M., Papamastorakis, J., Boumis, P., & Goudis, C. D. 2006, A&A, 459, 113. arXiv:astro-ph/0607638
Robitaille, T. P., & Whitney, B. A. 2010, ApJ, 710, L11. 1001.3672